Electronic Supplementary Information

for

In Situ Reversible Tuning of Chemical Interface Damping in Single Gold Nanorod-based Recyclable Platforms through Manipulation of Supramolecular Host–Guest Interactions

Hui Bin Jeon,[a] Sehoon Park,[a] Kyeong Rim Ryu,[a] Suman Kr Ghosh,[b] Jaehoon Jung,[a] Kyeng Min Park,[c] and Ji Won Ha[ad]*

[a]Department of Chemistry, University of Ulsan, 93 Daehak-ro, Nam-gu, Ulsan 44610, Republic of Korea

[b]Center for Self-Assembly and Complexity (CSC), Institute for Basic Science (IBS), Pohang, Gyeongsangbuk-do 37673, Republic of Korea

[c]Department of Biochemistry, School of Medicine, Daegu Catholic University, 33, 17-gil, Duryugongwon-ro, Nam-gu, Daegu 42472, Republic of Korea

[d]Energy Harvest-Storage Research Center (EHSRC), University of Ulsan, 93 Daehak-ro, Nam-gu, Ulsan 44610, Republic of Korea

*To whom correspondence should be addressed.

J. W. Ha

Phone: +82-52-712-8012

Fax: +82-52-712-8002

E-mail: jwha77@ulsan.ac.kr

<Table of Contents>

1. Experimental Section

1.1. Materials and Chemicals

CTAB-stabilized AuNRs were purchased from Nanopartz (Loveland, CO, USA). Oxaliplatin and spermine were purchased from American Type Culture Collection (Rockville, MD, USA). Highly purified water was produced by a Milli-Q Integral Water Purification System (18.2 MΩ cm^{-1}).

1.2. AuNR Characterization

The shape and size of AuNRs were characterized using an SEM microscope (JSM 6500, JEOL, Japan) operating at 10 kV and a TEM microscope (JEL 2100F, JEOL, Japan). UV–Vis extinction spectra for AuNRs were collected in a quartz absorption cell with a Varian Cary 300 UV–Vis spectrophotometer (Agilent, CA, USA). For UV–Vis measurements, the AuNR solution obtained from Nanopartz was used without dilution.

1.3. Synthesis of Cucurbit[7]uril (CB[7])

CB[7] used in this study was synthesized by a method previously reported by Kim an co-workers.[1] Glycoluril (5.68 g, 40.0 mmol) was suspended in 20 mL of 9M sulfuric acid in a 50 nL Erlenmeyer flask which was then heated to 70 °C in an oil bath. To the homogeneous solution was added formaldehyde (37% in water, 7.0 mL, 91 mmol). The mixture was stirred for 24 h while the temperature was maintained at 70-75°C. The temperature was raised to 95-100 °C and the mixture was further stirred for 12 h. During this period of time, sometimes crystalline CB[6] precipitated. The reaction mixture was poured into 200 mL of water. Acetone (1.0 L) was then added to the mixture to produce precipitate. After the mixture was allowed to stand for 15 min, the supernatant solution was removed by decantation. The remaining solid was further washed with 1:4 mixture of water/actone (1.0 L) twice. To the resulting solid was added a 1:1 mixture of water/acetone (200 mL). After a few min stirring, the mixture was filtered and washed

with water (100 mL) and dried under vacuum to yield a white powder containing mostly CB[6] (~4.0 g). Acetone (800 mL) was added to the filtrate and washing to produce precipitate which was filtered, washed with acetone and dried under vacuum to produce a mixture of mostly CB[5] and CB[7] in a ~1:1.5 ratio (1.42 g). The remaining solution contains CB[n] (n=8-11). The mixture of CB[5] and CB[7] was dissolved in water (75 mL) (with sonication if necessary). To the solution was added methanol (75 mL) to produce precipitate which was filtered, washed with methanol (10 mL) and dried under vacuum to yield a white powder containing mostly CB[7] (648 mg).

1.4. Synthesis of Monoamine-functionalized CB[7]

Monoamine-functionalized CB[7] was synthesized using a previously reported method.[2] Cysteamine hydrochloride (28 mg, 246.5 μmol) was added to the solution of monoallyloxy-CB[7] (30 mg, 24.6 μmol) dissolved in distilled water (1 mL). After purging with N_2, the mixture was irradiated with UV light (254 nm and 300 nm) for 16 h. The crude product was purified by washing with ethanol several times and finally dried in vacuum to yield monoamine-CB[7] (28 mg, 90 %).

1.5. Fabrication of a Flow Cell

A flow cell was fabricated using parafilm as a spacer between two coverslips #1 (24 mm × 60 mm). The channels were cut into the parafilm and holes were cut into one of the coverslips by using a commercially available CO_2-laser cutter system. The parafilm and coverslips were overlaid so that the holes in one of the coverslips matched with the ends of the channels in the parafilm. The flow cell was placed on a heating plate at 120 °C for a few seconds so that the parafilm melted and the flow cell became airtight.

1.6. Sample Preparation for Single-Particle Microscopy and Spectroscopy

The samples for single-particle studies were prepared as follows. First, the colloidal solution was diluted with 18.2-MΩ pure water to the proper concentration. Then, the diluted solution was sonicated for 10 min at room temperature. The samples were prepared by drop casting the diluted AuNR solution onto a pre-cleaned glass slide. Then, this slide was covered with a 22 mm × 22 mm No. 1.5 coverslip (Corning, NY, USA). Throughout all experiments, the area density of AuNRs deposited on the glass slide was maintained at approximately 1.0 μm^{-2} to facilitate single-AuNR characterization, free of inter-particle interactions and LSPR coupling.

1.7. Single-Particle DF Microscopy and Spectroscopy

DF microscopy imaging was conducted on an in-house system comprising a Nikon inverted microscope (ECLIPSE Ti-U, Japan), a CCD camera (iXon Ultra 897, UK), and image analysis software. In the DF mode, we used a Nikon Plan Fluor 100 × 0.5–1.3 oil iris objective and a Nikon DF condenser. A 100W halogen lamp was used as the illumination source. The Andor iXon^{EM}+ CCD camera acquired the DF scattering images of AuNRs. The collected images were then analyzed using the ImageJ software. Furthermore, the DF scattering spectra were acquired using an Andor spectrometer (SHAMROCK 303i, SR-303I-A, UK) and an Andor CCD camera (Newton DU920P-OE, UK). For the analysis, the scanning stage was positioned to present the sample at the desired location. Therefore, only the scattered light from the selected location was collected by the objective. The scattered light was directed to the spectrometer, dispersed by a grating (300 lines/mm), and detected by a Newton CCD camera (Andor, UK). The background spectrum was obtained from the region without particles.

1.8. Correlation Study between SEM and Optical Microscopy

In this study, we correlated SEM images with optical images and spectra of single Au nanoparticles (AuNRs, Fig. 1). After cleaning glass slides, a gold pattern was created by evaporating a 5 nm Ti layer followed by a 20 nm Au layer through an indexed copper Transmission Electron Microscopy (TEM) grid (Ted Pella) placed on the cleaned glasses (Fig. S6). This pattern aided in locating the same particles in SEM and optical microscopy as clearly demonstrated in the overlaid SEM and DF image. First, we took SEM images of single Au nanoparticles well separated on a glass slide. We then obtained DF scattering images and spectra of same Au nanoparticles under DF microscopy and spectroscopy.

1.9. Real-Time Binding Experiments under DF Single Particle Spectroscopy

Single particle scattering spectra of Au nanoparticles were obtained at the start of the experiment for reference. Then, a solution of adsorbate molecules (e.g., CB[7]-NH_2, oxt@CB[7]-NH_2, spm@CB[7]-NH_2) was introduced through the flow cell while continuously taking single particle spectra of the same AuNRs for a period of 60 min with 3 min intervals. It should be noted that amine (-NH_2) group has a strong affinity for gold.

1.10. NMR Spectroscopic Measurements

The host-guest complex of oxaliplatin in CB[7] (oxt@CB[7]) was prepared by following the procedure as reported elsewhere. To see the effect of competitors, NaCl (58 mg), spermine hydrochloride (7 mg) or FcA (11 mg) was added to a solution of oxt@CB[7] in D_2O (1 mL) after filtering through a syringe filter (Nylon, 0.45 μm).

1.11. Langmuir Adsorption Isotherm

In this study, to compare quantitatively the amount of CID when introducing various adsorbate molecules, it was necessary to establish whether a comparable, if not complete, coverage of

adsorbed molecules had been achieved.[3] Therefore, a time evolution typical for a Langmuir adsorption isotherm was employed, i.e., $\theta = 1-\exp(-k_L \cdot c \cdot t)$, where the coverage θ depends on the time t, thiol concentration c, and Langmuir adsorption constant k_L. As the concentration of adsorbated molecules was constant, the adsorption constant was simplified to $k = k_L \cdot c$ and the LSPR linewidth broadening due to adsorption was fitted with $\Delta\Gamma(t) = \Delta\Gamma_{CID}[1-\exp(-kt)]$.[3] This Langmuir adsorption model led to the equilibrium value of CID, $\Delta\Gamma_{CID}$, for AuNRs at complete adsorption. These $\Delta\Gamma_{CID}$ values compare well with the LSPR linewidth broadening measured for individual nanoparticles after 60 min of adsorbate binding.

1.12. Defocused Orientation and Position Imaging Technique

Anisotropic AuNRs that are much smaller than the wavelength of incident light can be considered electric point dipoles. According to an electrostatic approximation, plasmon oscillations from anisotropic AuNR can be simplified as three-perpendicular independent dipoles along the three axes (Fig. S10). Oscillation along the long principal axis (a-axis) is defined as a longitudinal mode and the other perpendicular oscillations are defined as transverse modes vibrating along the short axes (b and c axes). E_a indicates the scattering electric field of the AuNR along the main long axis, while E_b and E_c are the scattering electric fields along the short transverse axes, b and c. The overall scattering electrical field from a AuNR can be quantified through a linear superposition of three independent scattering electric fields associated with three mutually orthogonal dipoles, as shown in the following equation:

$$E_{(scat)} = \sum_{a,b,c} E_{(scat)j} = E_{(scat)a} + E_{(scat)b} + E_{(scat)c}$$

However, E_a the scattering electric field of the AuNR along the main long axis (or the longitudinal dipole) is much more dominant than the two transverse dipoles. Therefore, a AuNR behaves as a single dipole character.

Defocused orientation and position imaging (DOPI) technique[4] is a direct and simple method with the capability of visualizing and determining three-dimensional (3D) dipole orientation of anisotropic single AuNRs. The core idea is that the direct detection of the spatial distribution of the scattered or emitted field of single dipoles becomes possible when the imaging system is defocused deliberately by ~1 μm.

1.13. Simulation of Scattering Image Patterns of AuNRs

We used the simulation program developed by Enderlein and Böhmer.[5] The program is designed to calculate the characteristic intensity distribution from an emitter with three perpendicular emission dipoles of different emission strength. It has been widely used to determine the spatial orientation of single dye molecules.[5, 6] The simulation program is a special Matlab based utility with a graphics user interface (GUI) for easy calculation. This program allows us to calculate exactly the defocused (or focused) images of single molecules. For using the GUI, one should download the files from the website (http://www.joerg-enderlein.de/imagingOfSingleMolecules.html).

The parameters that can be input are: the numerical aperture of the objective lens, magnification of imaging, extent of defocusing (or defocusing distance in micrometers), κ and R. For defining the emission strength ratios of the three independent dipoles (Fig. S10), we input the parameter κ and R into the program. The ratio κ defines the ratio of the emission strength of the b- to the c-dipole (transverse dipoles, Fig. S10) as shown below.

$$I_b / I_c = (1-\kappa)/(1+\kappa)$$

In addition, the ratio R defines the emission strength of the a-dipole (or longitudinal dipole) to the combined b and c dipoles (or transverse dipoles) as shown below.

$$R \times I_a + (1-R) \times (I_b + I_c)$$

When *R* is 1, we only have the contribution from *a*-dipole (longitudinal dipole) to the image patterns. In the present study, we used a *R* value of 1 to simulate the scattering patterns of single dipoles generated on the AuNR surface at different LSPR excitation wavelengths.

1.14. Multiple Orientation Effect of Single AuNRs

In CID studies using single AuNRs, their orientations on a glass slide could also affect the experimental results. Therefore, this study investigated the 3D spatial orientations of single AuNRs cast on a glass slide through DF scattering imaging, as shown in Figs. S11 and S12. When the DF images were defocused, certain patterns could be observed like a donut-shape, indicating the orientation (or spatial field distribution) of a particle by the brightness (Figs. S11 and S12).[4, 7-9] To increase the degree of confidence, a simulation was performed, which produced results consistent with the experimental results (Fig. S12). From the defocused DF imaging method, we found that a majority of AuNRs are lying almost flat to the glass slide when casted on it. However, we also found that some AuNRs showed asymmetric doughnut patterns with a ring opening, which means they are tilted from a horizontal plane. As shown in Figs. S11B and S12B, two AuNRs have the polar angle, θ, of 74° and 68°. Therefore, we ensured that there is no effect of orientation for the CID experiment of AuNRs while focusing only on the chemical effect.

1.15. Computational Study

The self-consistent tight-binding (GFN2-xTB) method[10] was utilized for optimizing various inclusion complexes, and then the hybrid PBE0 functional[11] implemented in the Gaussian 16 software package[12] was employed to more precisely evaluate their energy values and electronic structures. To effectively describe the dispersive interaction, Grimme's D4[13] and D3[14] methods

were used for GFN2-xTB and PBE0 calculations, respectively. The LanL2DZ effective pseudo-potential was used for the basis set for Pt,[15] and the 6-31++G(d,p) was used for other elements in PBE0-D3 calculations. The influence of solvent (water) medium was also considered using the COSMO[16] and IEFPCM[17] methods for GFN2-xTB and PBE0 calculations, respectively.

1.16. Lorentzian Fitting of Single Particle Scattering Spectra

The DF scattering spectra of single AuNRs were fitted to a Lorentzian function, $I(\omega) = C_0 / [(\omega - \omega_0)^2 + \Gamma^2 / 4]$, to determine the LSPR linewidth Γ and the resonance frequency ω_0. The LSPR line-shape can be affected by interband transition (i.e., LSPR energy above 1.7 eV). However, as shown in Figs. 1C and S8, the experimental scattering spectra of single AuNRs were well fitted with a Lorentzian function in the energy range.

2. References

1. J. Kim, I.-S. Jung, S.-Y. Kim, E. Lee, J.-K. Kang, S. Sakamoto, K. Yamaguchi and K. Kim, *Journal of the American Chemical Society*, 2000, **122**, 540-541.
2. Y. Ahn, Y. Jang, N. Selvapalam, G. Yun and K. Kim, *Angewandte Chemie International Edition*, 2013, **52**, 3140-3144.
3. B. Foerster, A. Joplin, K. Kaefer, S. Celiksoy, S. Link and C. Sönnichsen, *ACS Nano*, 2017, **11**, 2886-2893.
4. E. Toprak, J. Enderlein, S. Syed, S. A. McKinney, R. G. Petschek, T. Ha, Y. E. Goldman and P. R. Selvin, *Proceedings of the National Academy of Sciences*, 2006, **103**, 6495-6499.
5. M. Böhmer and J. Enderlein, *J. Opt. Soc. Am. B*, 2003, **20**, 554-559.
6. M. A. Lieb, J. M. Zavislan and L. Novotny, *J. Opt. Soc. Am. B*, 2004, **21**, 1210-1215.
7. L. Xiao, Y. Qiao, Y. He and E. S. Yeung, *Analytical Chemistry*, 2010, **82**, 5268-5274.
8. L. Wei, J. Xu, Z. Ye, X. Zhu, M. Zhong, W. Luo, B. Chen, H. Duan, Q. Liu and L. Xiao, *Analytical Chemistry*, 2016, **88**, 1995-1999.
9. J. W. Ha, K. Marchuk and N. Fang, *Nano Letters*, 2012, **12**, 4282-4288.
10. C. Bannwarth, S. Ehlert and S. Grimme, *Journal of Chemical Theory and Computation*, 2019, **15**, 1652-1671.
11. C. Adamo and V. Barone, *The Journal of Chemical Physics*, 1999, **110**, 6158-6170.
12. M. J. Frisch, G. W. Trucks, H. B. Schlegel, G. E. Scuseria, M. A. Robb, J. R. Cheeseman, G. Scalmani, V. Barone, G. A. Petersson, H. Nakatsuji, X. Li, M. Caricato, A. V. Marenich, J. Bloino, B. G. Janesko, R. Gomperts, B. Mennucci, H. P. Hratchian, J. V. Ortiz, A. F. Izmaylov, J. L. Sonnenberg, Williams, F. Ding, F. Lipparini, F. Egidi, J. Goings, B. Peng, A. Petrone, T. Henderson, D. Ranasinghe, V. G. Zakrzewski, J. Gao, N. Rega, G. Zheng, W. Liang, M. Hada, M. Ehara, K. Toyota, R. Fukuda, J. Hasegawa,

M. Ishida, T. Nakajima, Y. Honda, O. Kitao, H. Nakai, T. Vreven, K. Throssell, J. A. Montgomery Jr., J. E. Peralta, F. Ogliaro, M. J. Bearpark, J. J. Heyd, E. N. Brothers, K. N. Kudin, V. N. Staroverov, T. A. Keith, R. Kobayashi, J. Normand, K. Raghavachari, A. P. Rendell, J. C. Burant, S. S. Iyengar, J. Tomasi, M. Cossi, J. M. Millam, M. Klene, C. Adamo, R. Cammi, J. W. Ochterski, R. L. Martin, K. Morokuma, O. Farkas, J. B. Foresman and D. J. Fox, *Journal*, 2016.

13. E. Caldeweyher, S. Ehlert, A. Hansen, H. Neugebauer, S. Spicher, C. Bannwarth and S. Grimme, *The Journal of Chemical Physics*, 2019, **150**, 154122.
14. S. Grimme, J. Antony, S. Ehrlich and H. Krieg, *The Journal of Chemical Physics*, 2010, **132**, 154104.
15. P. J. Hay and W. R. Wadt, *The Journal of Chemical Physics*, 1985, **82**, 299-310.
16. A. Klamt and G. Schüürmann, *Journal of the Chemical Society, Perkin Transactions 2*, 1993, DOI: 10.1039/P29930000799, 799-805.
17. G. Scalmani and M. J. Frisch, *The Journal of Chemical Physics*, 2010, **132**, 114110.

3. Supplementary Figures

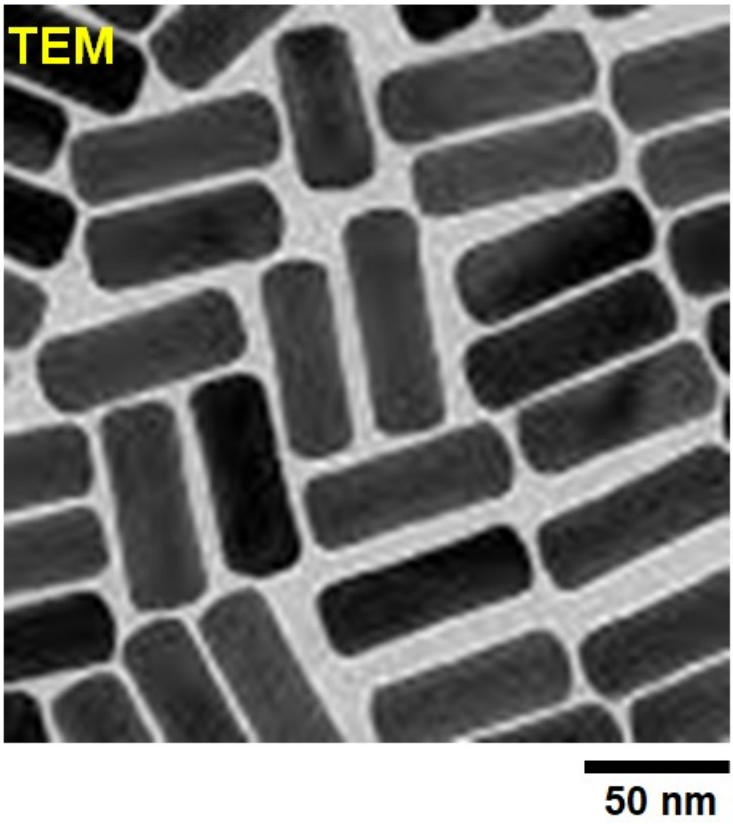

Fig. S1 TEM image of AuNRs used in this study, purchased from Nanopartz.

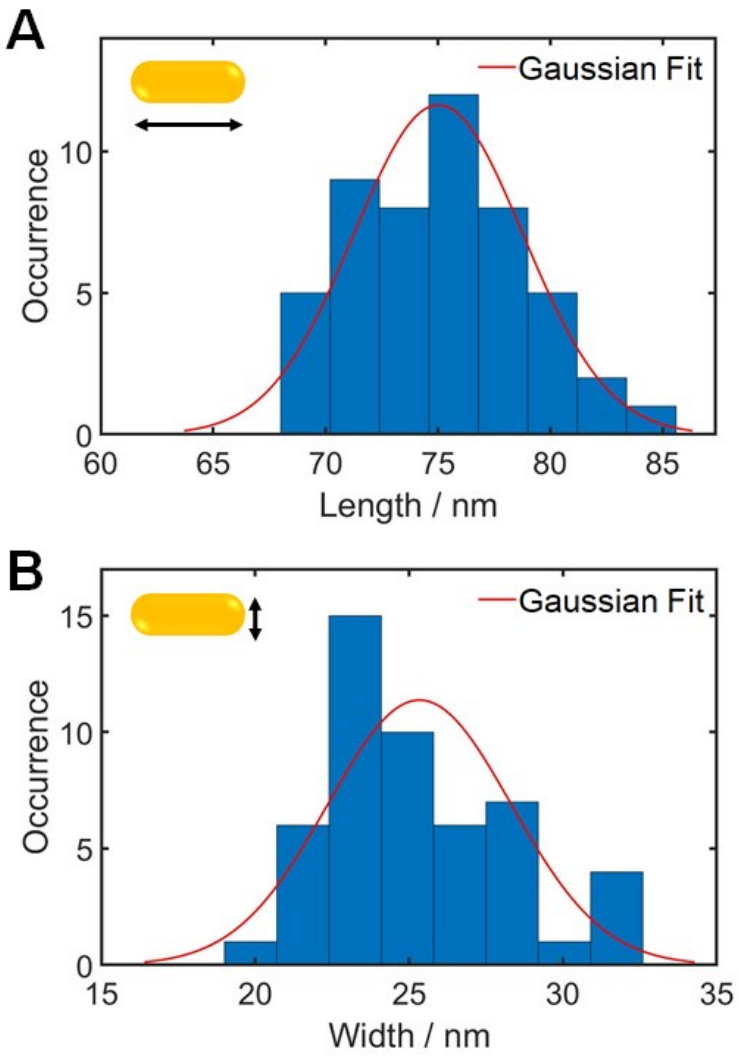

Fig. S2 Histograms to show the average length **(A)** and width **(B)** of single AuNRs used in this study. A red-curve shows a Gaussian fit to the experimental data, yielding the mean length and width. Their mean sizes were determined to be 25.1(±2.78) nm × 75.4(±3.53) nm.

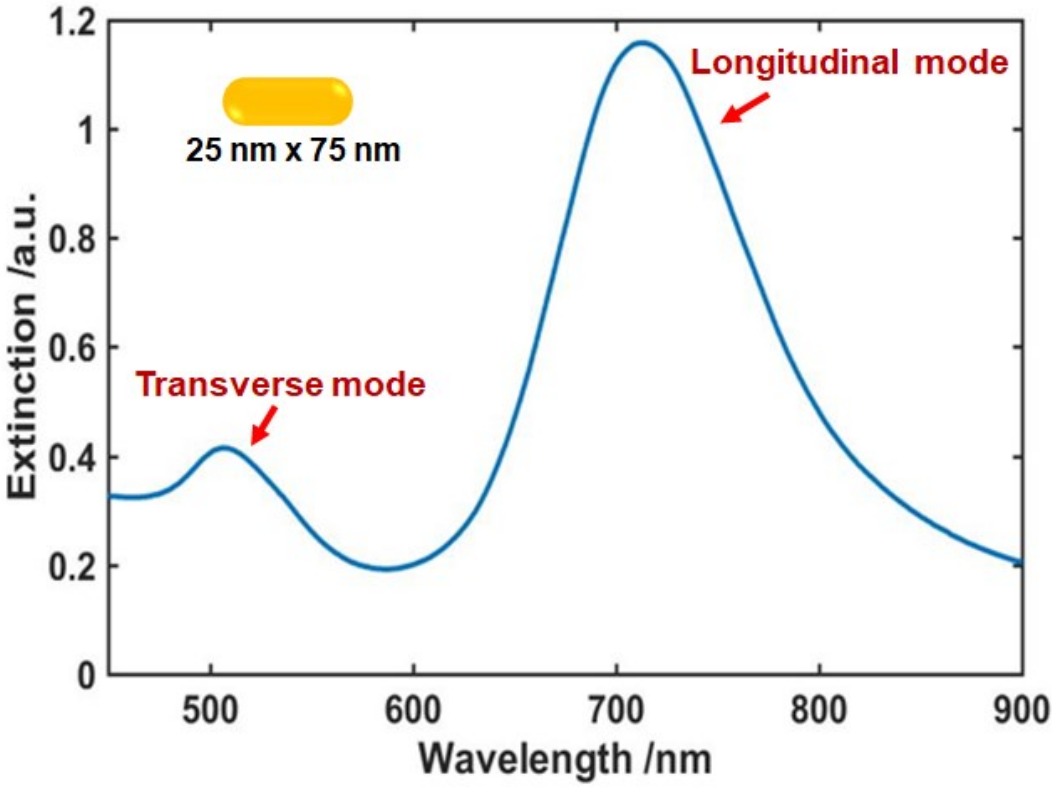

Fig. S3 UV-Vis extinction spectrum of AuNRs dispersed in water. Two transverse and longitudinal LSPR peaks are observed at 522 nm and 713 nm, respectively.

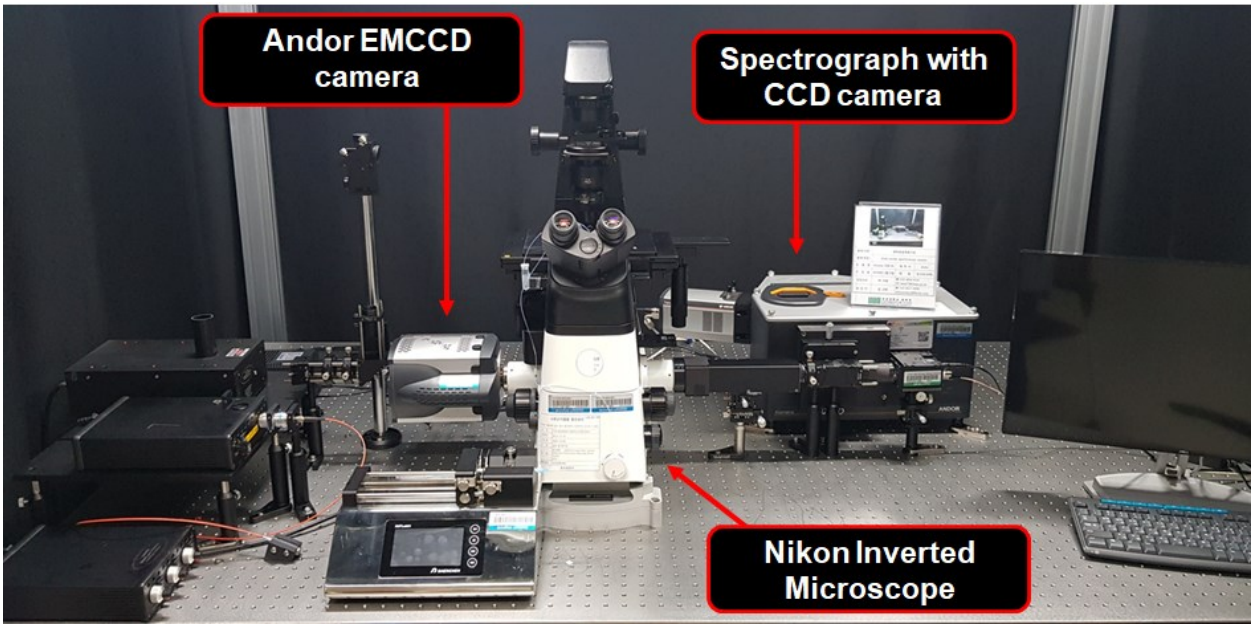

Fig. S4 A photograph to show the experimental setup for single particle microscopy and spectroscopy.

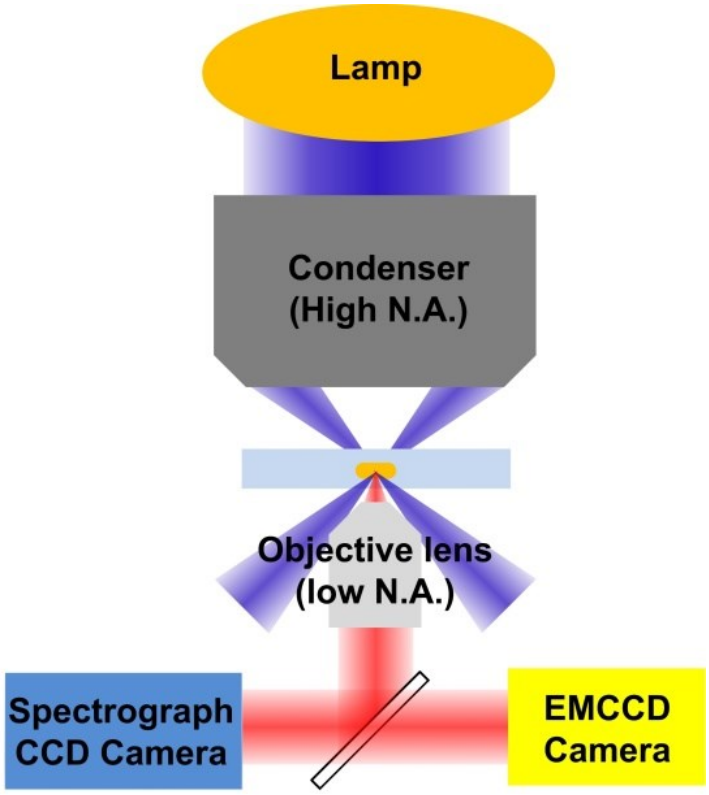

Fig. S5 Schematic diagram to show the working principle of scattering-based DF microscopy and spectroscopy for single AuNRs.

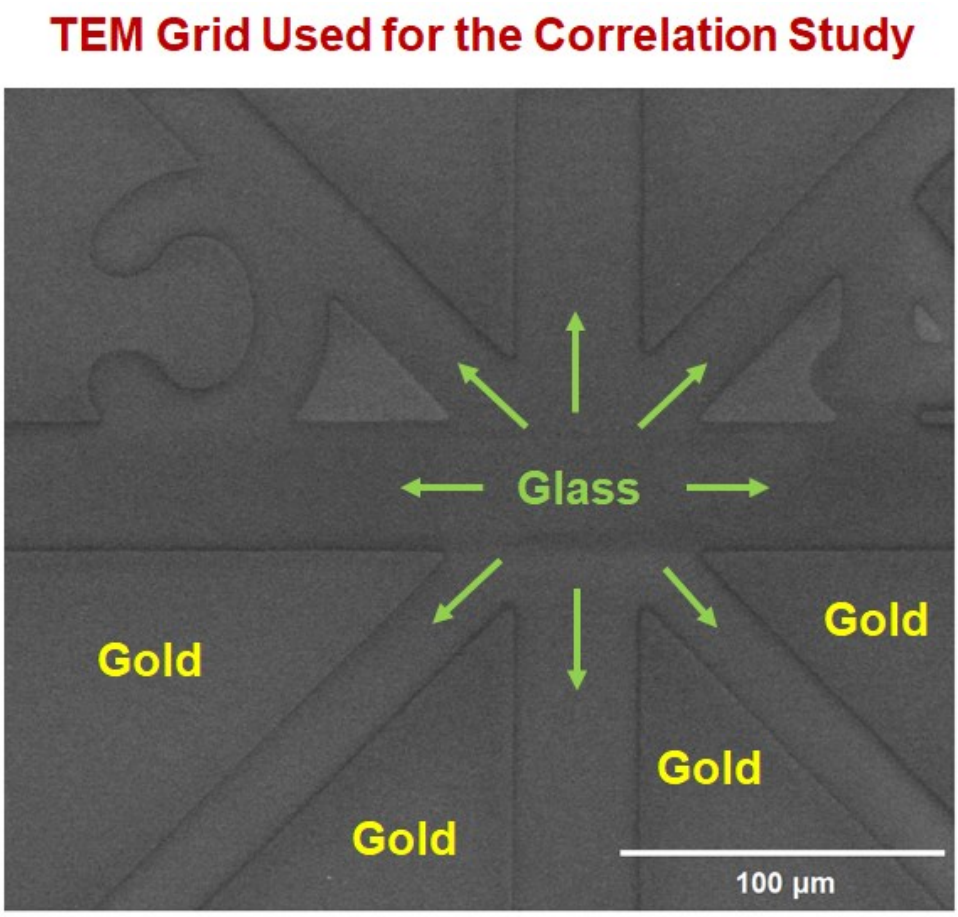

Fig. S6 A sample patterned with a TEM grid used in the correlation study of single AuNRs. The gold pattern allowed to locate same AuNRs under optical microscopy.

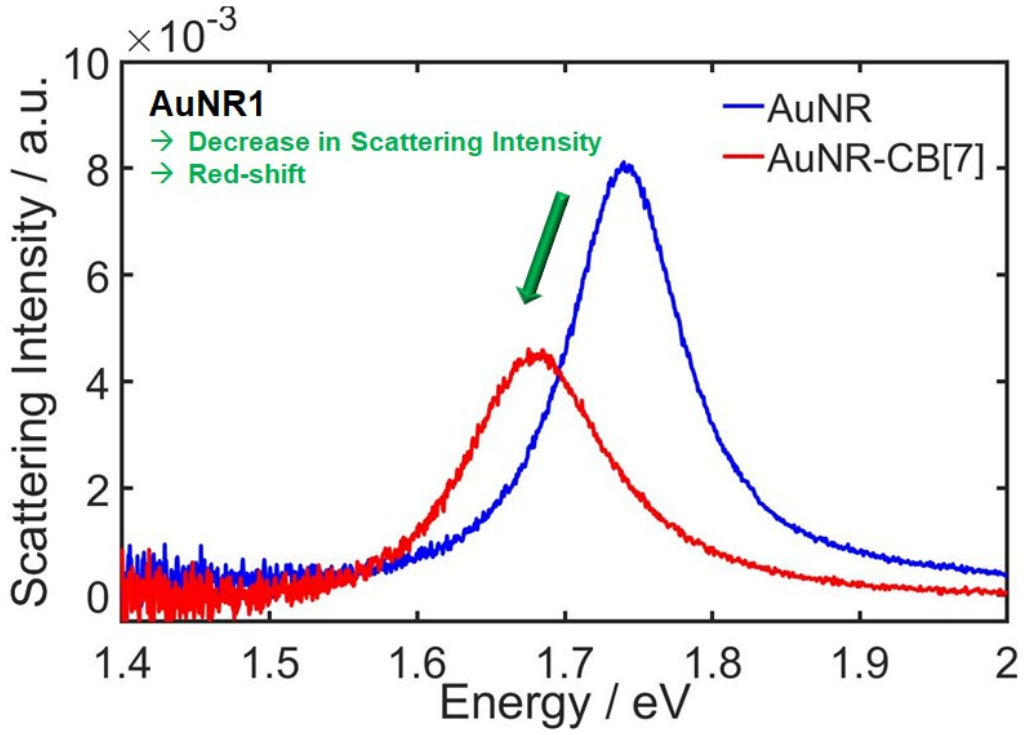

Fig. S7 Single particle scattering spectra of AuNR1 in Fig. 1B recorded in water before the adsorption of CB[7]-NH_2 and 60 minutes after the adsorption of CB[7]-NH_2. A decrease in the scattering intensity is observed, indicated by a green-arrow.

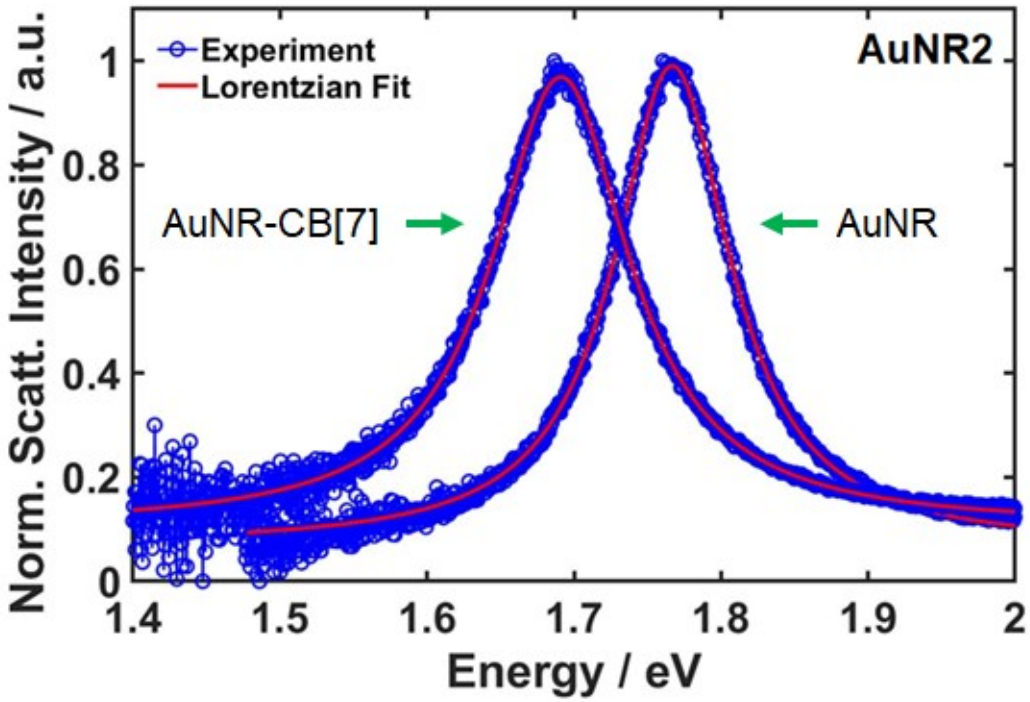

Fig. S8 Single particle scattering spectra of AuNR2 in Fig. 1B recorded in water before the adsorption of CB[7]-NH_2 and 60 minutes after the adsorption of CB[7]-NH_2. Single particle scattering spectra were normalized to better compare the LSPR wavelength shift as well as the LSPR linewidth broadening.

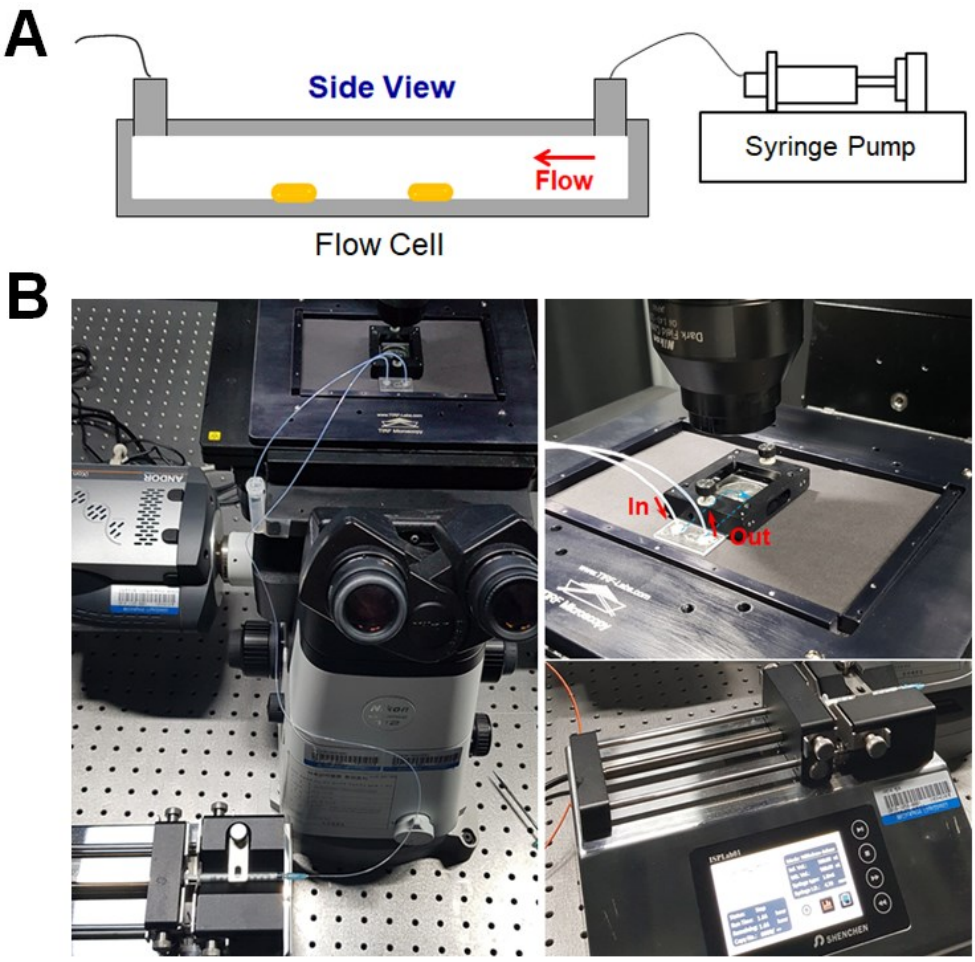

Fig. S9 (A) Schematic to show a flow cell used in this study. **(B)** Photograph to show the experimental setup of an optical microscope with a flow cell and a syringe pump.

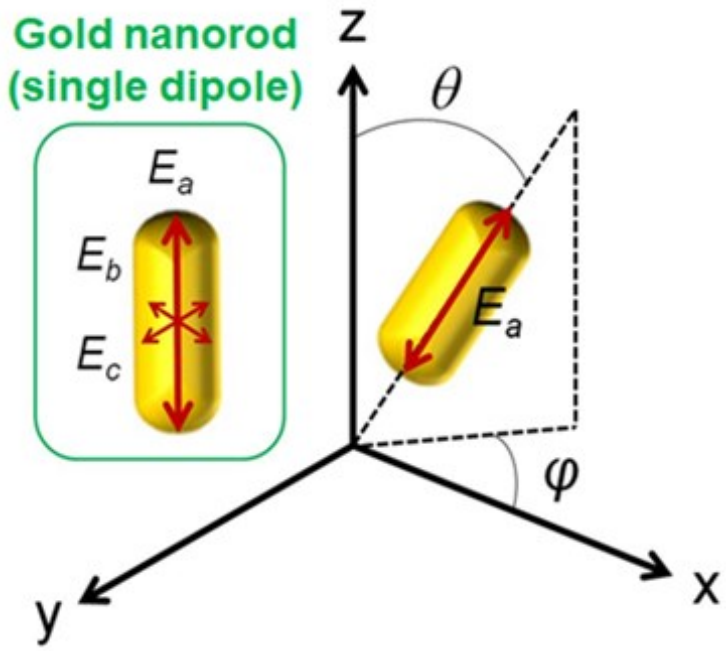

Fig. S10 Schematic depicting three-perpendicular dipoles along the three axes. E_a denotes the scattering electric-field of the AuNR along the main long axis. Definitions of the polar angle θ and the azimuthal angle φ of a AuNR in 3D space are also shown.

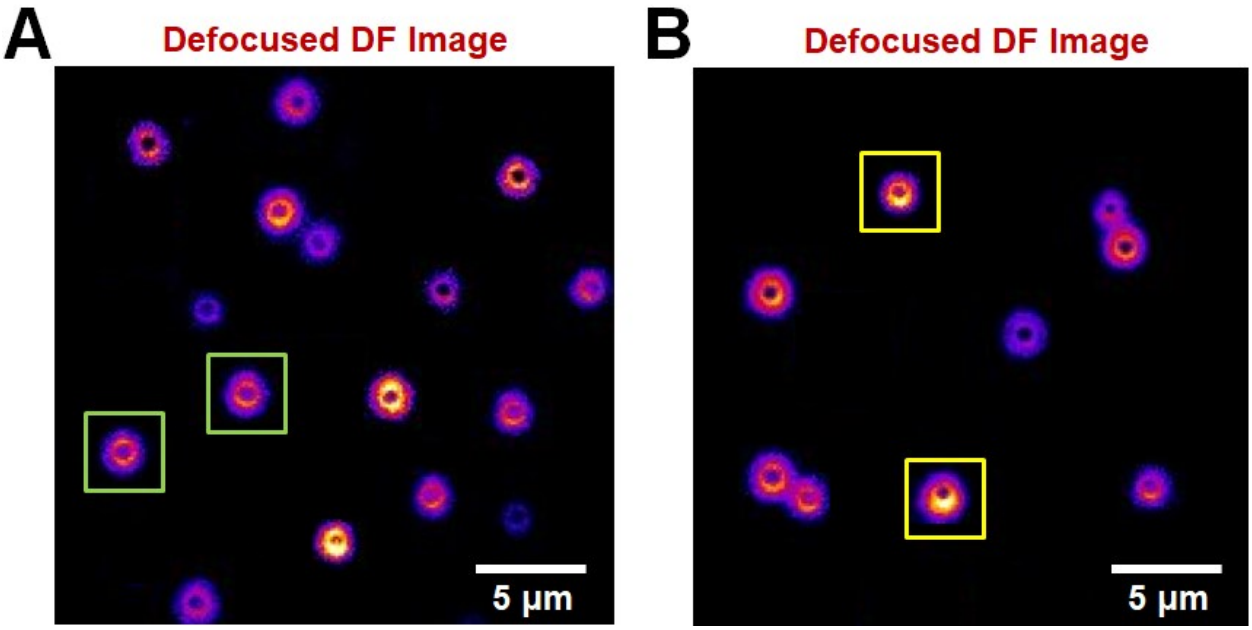

Fig. S11 (A) Defocused scattering image of single AuNRs deposited on a glass slide. A donut-shaped image pattern is observed for AuNRs. Most AuNRs showed symmetrical image patterns without a ring opening. **(B)** Defocused scattering image of single AuNRs. A few AuNRs squared with a yellow showed asymmetric doughnut patterns with a ring opening. We can extract 3D spatial orientations of single AuNRs from their characteristic doughnut-shaped scattering patterns.

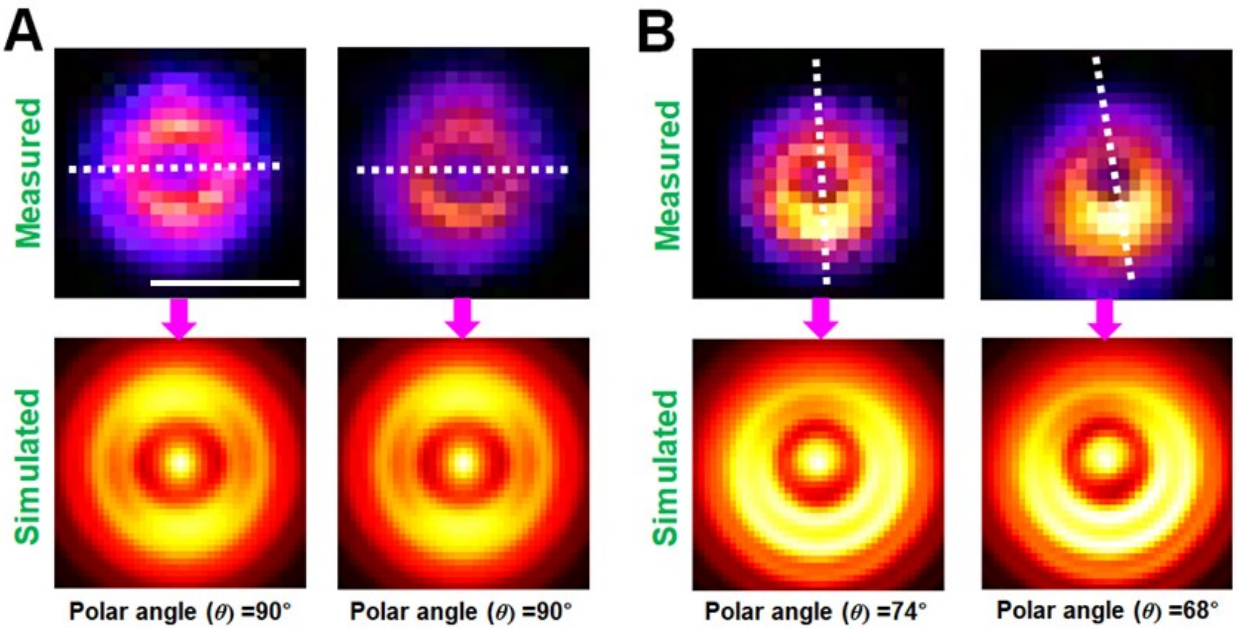

Fig. S12 The measured and best-matched simulation patterns from randomly selected AuNRs (Fig. S11). **(A)** The measured and simulated defocused patterns for the two AuNRs squared with a green color in Fig. S11A with the polar angle of ~90°. The scale bar indicates 1 μm. **(B)** The measured and simulated defocused patterns for the two AuNRs squared with a yellow color in Fig. S11B. Asymmetric ring opening is observed in the defocused patterns, meaning that the AuNRs are tilted from the horizontal plane. It is shown that the measured patterns match well with the simulated patterns.

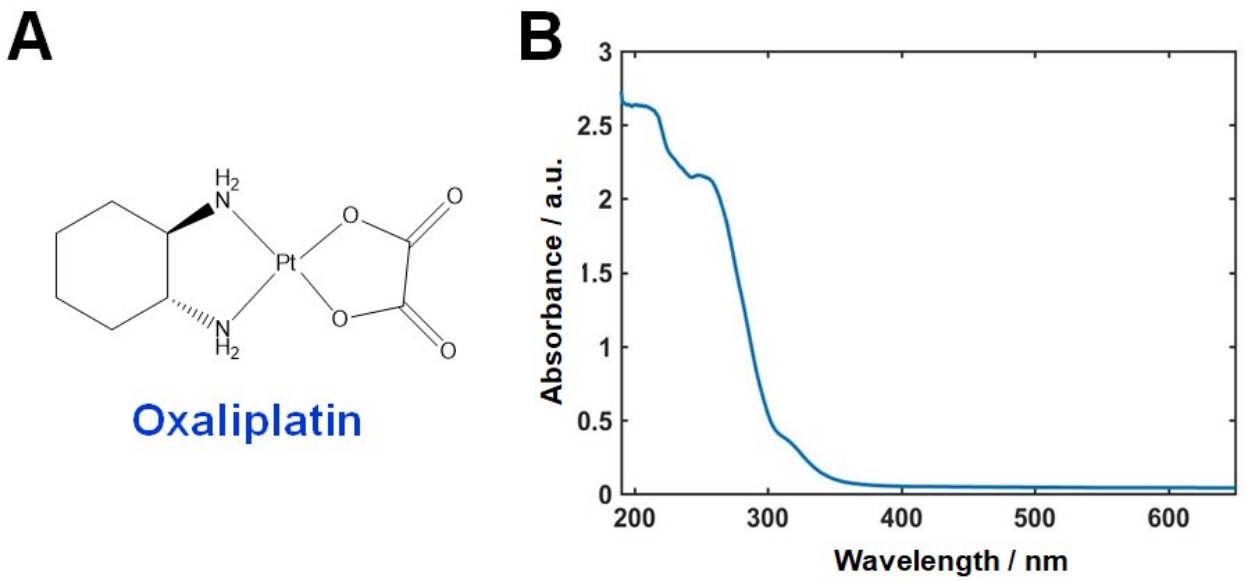

Fig. S13 (A) Chemical structure of oxaliplatin used as guest for CB[7] in this study. **(B)** UV-Vis absorption spectrum of oxaliplatin dissolved in water.

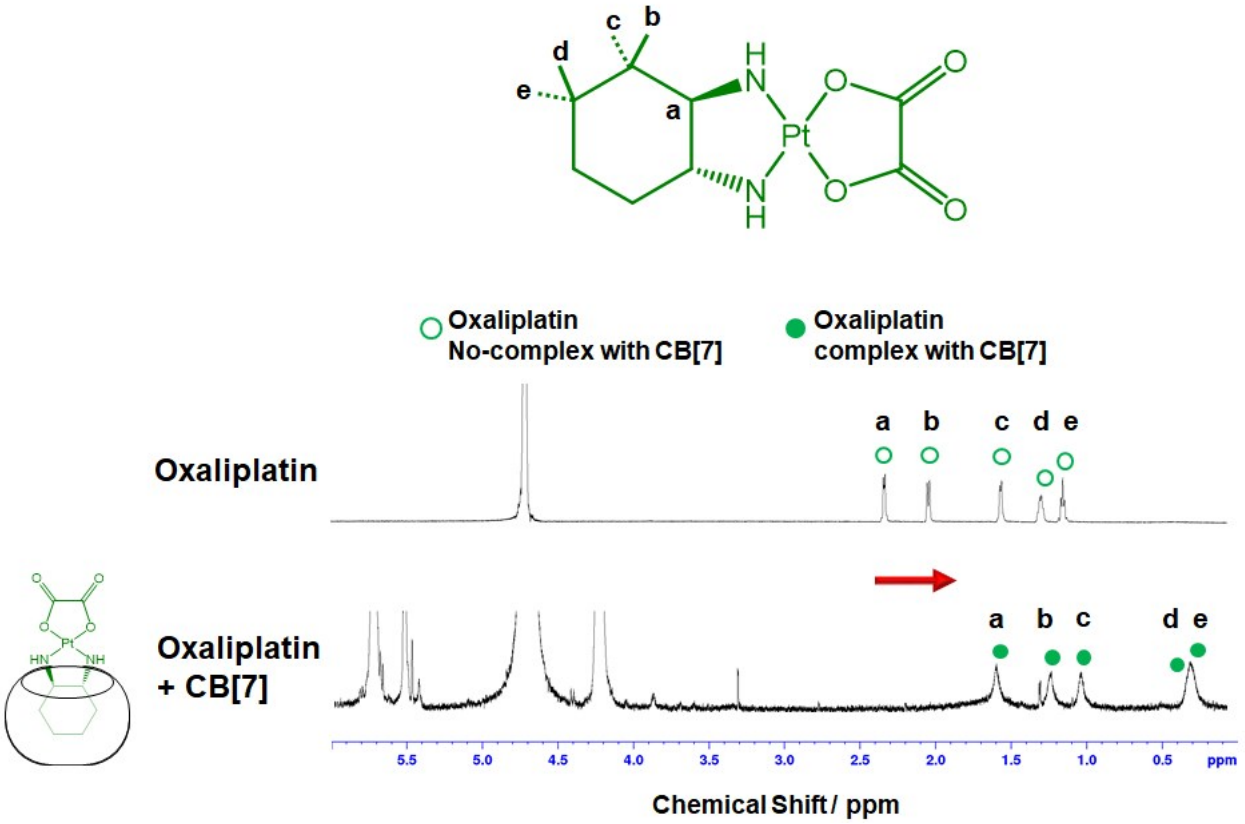

Fig. S14 The ^{1}H NMR spectroscopic study. The formation of the oxt@CB[7] inclusion complex was confirmed by ^{1}H NMR spectroscopic measurements. All the peaks (a-e) for the cyclohexyl ring protons of the guest are shifted upfield relative to those of the free guest (oxaliplatin), indicating that the cyclohexyl ring is located inside the cavity of CB[7].

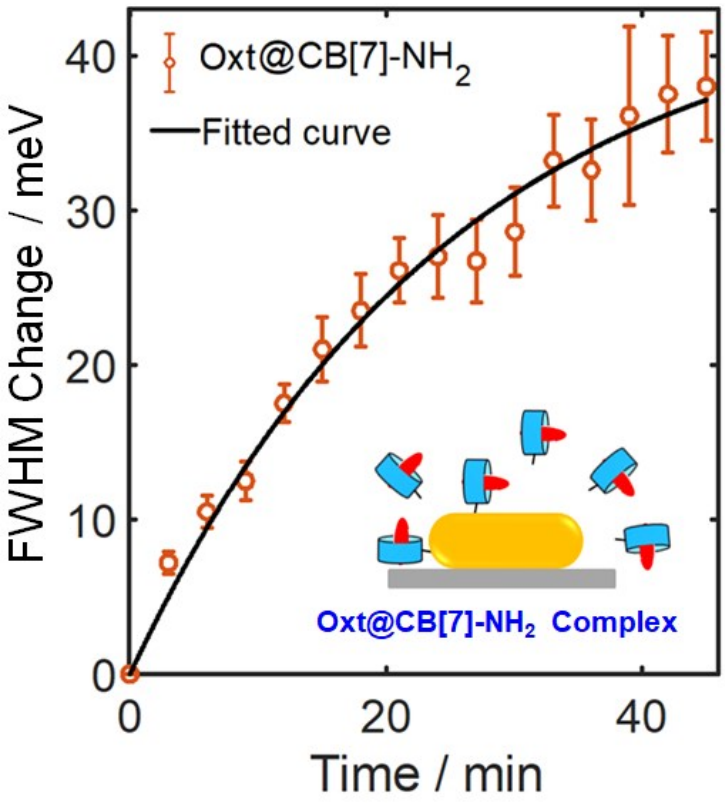

Fig. S15 Time dependence of the adsorption of oxt@CB[7]-NH_2 observed *via* LSPR linewidth (or FWHM) broadening for single AuNRs. The scattering spectra of 50 single AuNRs were obtained repeatedly for a period of approximately 60 min and the LSPR linewidth $\Delta\Gamma$ was extracted with respect to the starting value. The fitted curves are shown as black. The presented kinetics of FWHM change (or CID) is an average of 50 single AuNRs and the error bars are their standard deviations.

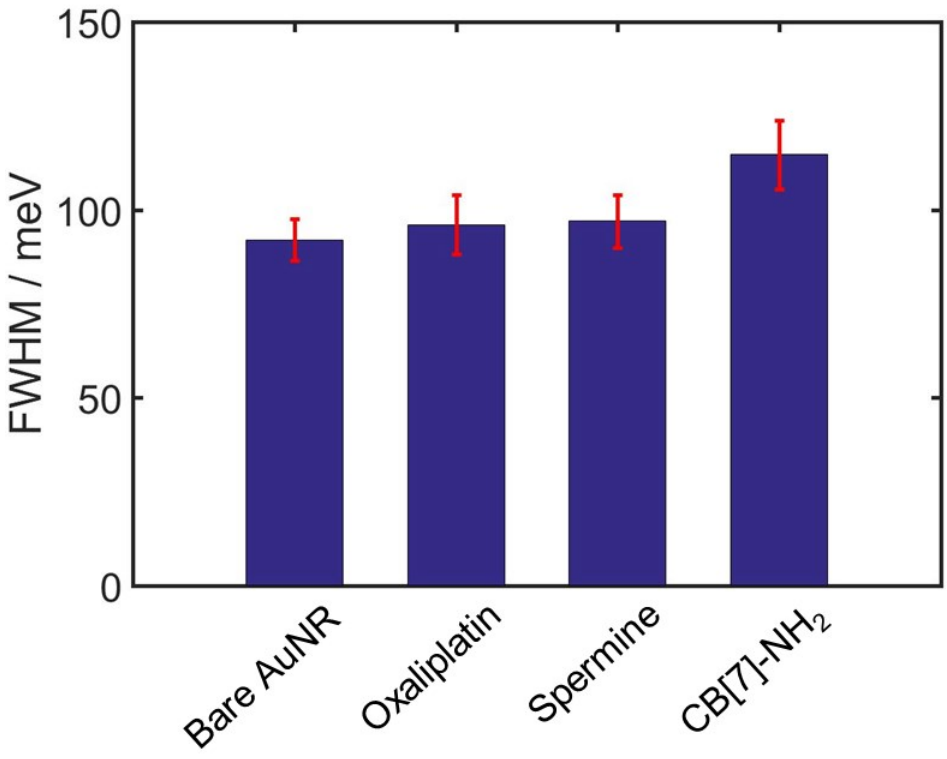

Fig. S16 Effect of nonspecific adsorption of the guest on the linewidth broadening (or FWHM). Comparison of the linewidth broadening induced by the adsorption of oxaliplatin, spermine, and CB[7]-NH_2. The FWHM value induced by the guest (oxaliplatin and spermine) was comparable to that of bare AuNR. In contrast to nonspecific adsorption of the guest, there was a significant change in the FWHM value induced by specific adsorption of CB[7]-NH_2 on the AuNR surfaces.

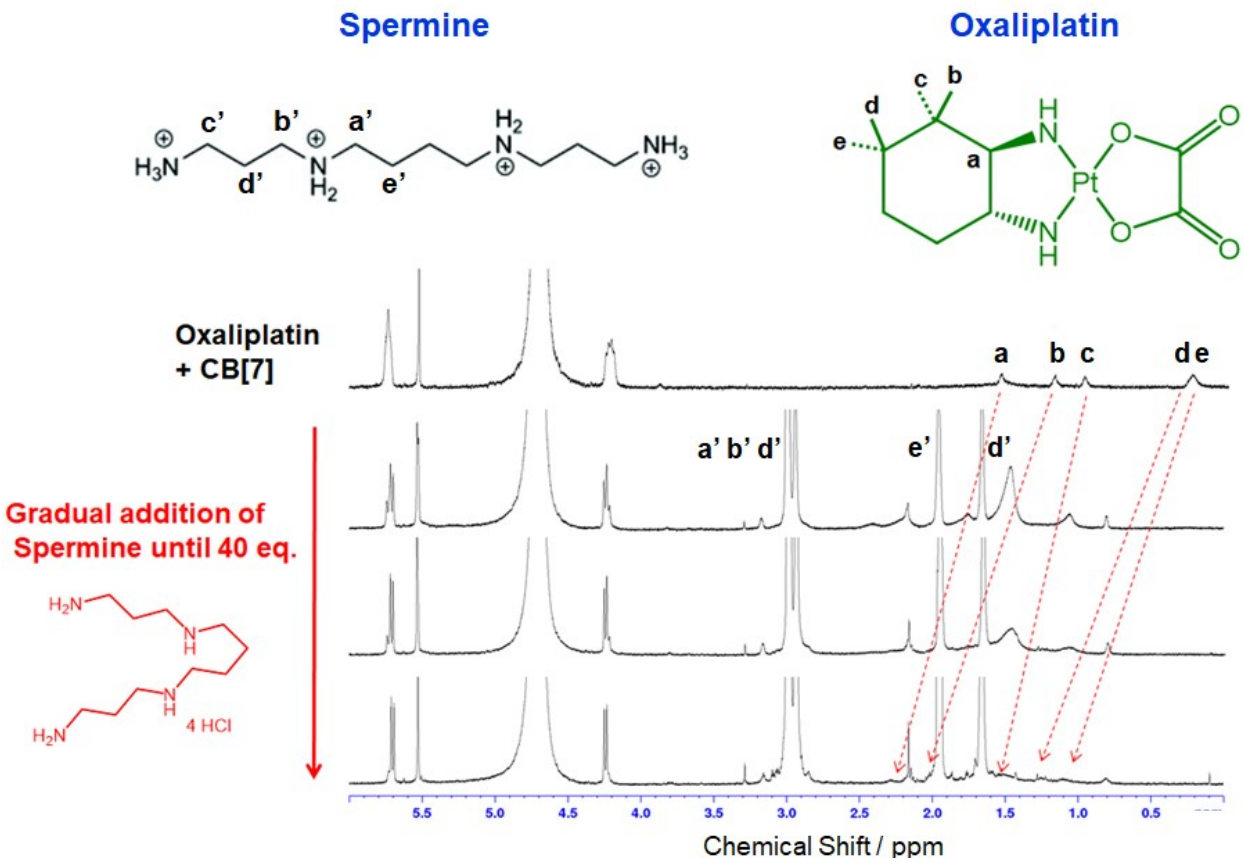

Fig. S17 The ^{1}H NMR spectroscopic measurements were performed to confirm the competitive replacement process by spermine. The protons of 1,2-diaminocyclohexane as the ligand of oxaliplatin showed significant upfield shifts after its complexation with CB[7], indicating that the 1,2-diaminoyclohexane group is incorporated into CB[7]. Spermine was then quantitatively added into the oxt@CB[7]-NH_2 complex at the ratios of 10.0, 20.0, and 40.0 eq. With the increase in the amount of spermine, the NMR signals (a-e) of the protons of 1,2-diaminocyclohexane on oxaliplatin gradually decreased and shifted downfield to the peak positions of oxaliplatin only, indicating a dynamic exchange of oxaliplatin and spermine in the cavity of CB[7] and the release of oxaliplatin by spermine

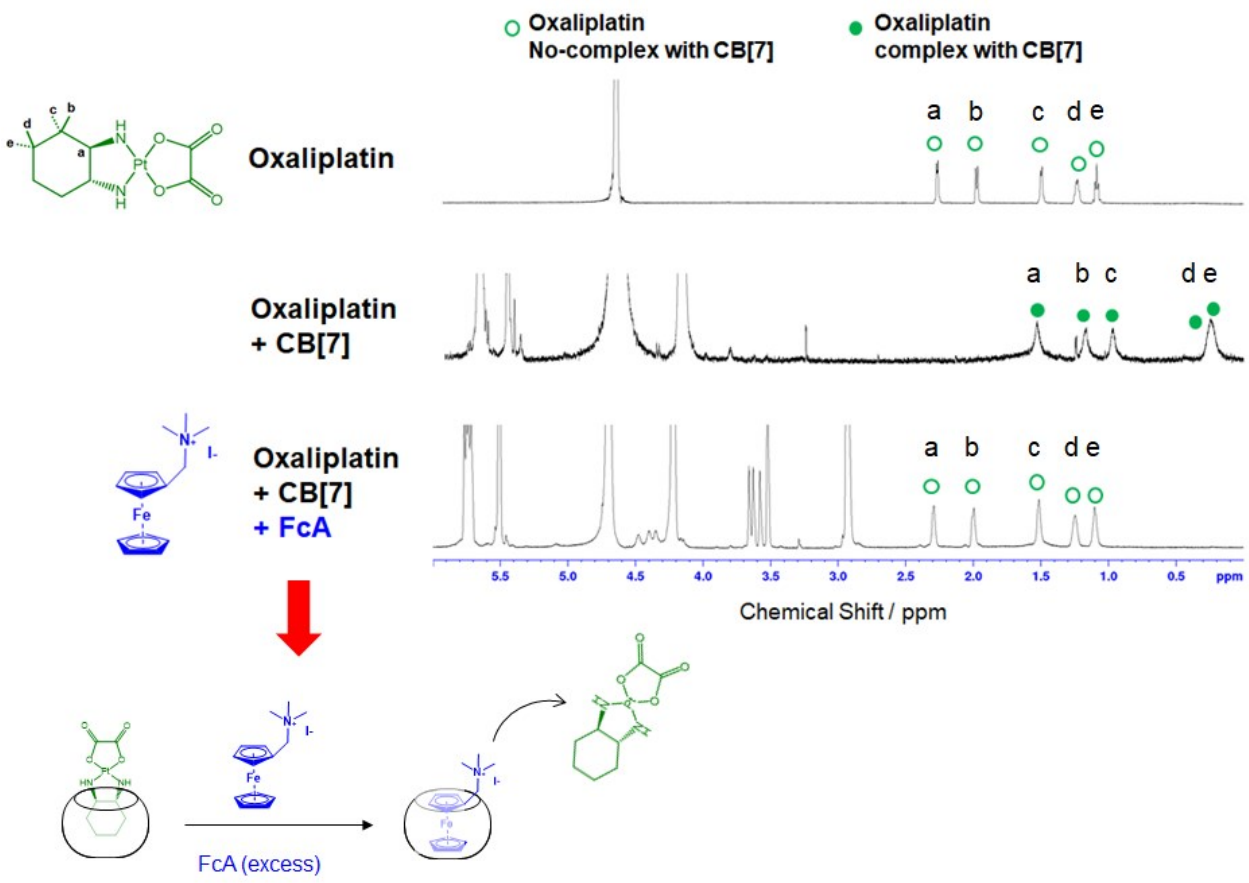

Fig. S18 The ^{1}H NMR spectroscopic measurements were performed to confirm the capability of competitive replacement of oxaliplatin form oxt@CB[7] complex by a competitive guest FcA with the most strongest binding constant (K_a of $10^{12.6}$ M^{-1} in water). The protons of 1,2-diaminocyclohexane as the ligand of oxaliplatin showed significant upfield shifts after its complexation with CB[7], indicating that the 1,2-diaminoyclohexane group is incorporated into CB[7]. By the addition of FcA, NMR signals (a-e) of the protons of 1,2-diaminocyclohexane on oxaliplatin shifted downfield to the peak positions of oxaliplatin only, indicating a dynamic exchange of oxaliplatin and FcA in the cavity of CB[7] and the release of oxaliplatin by FcA.

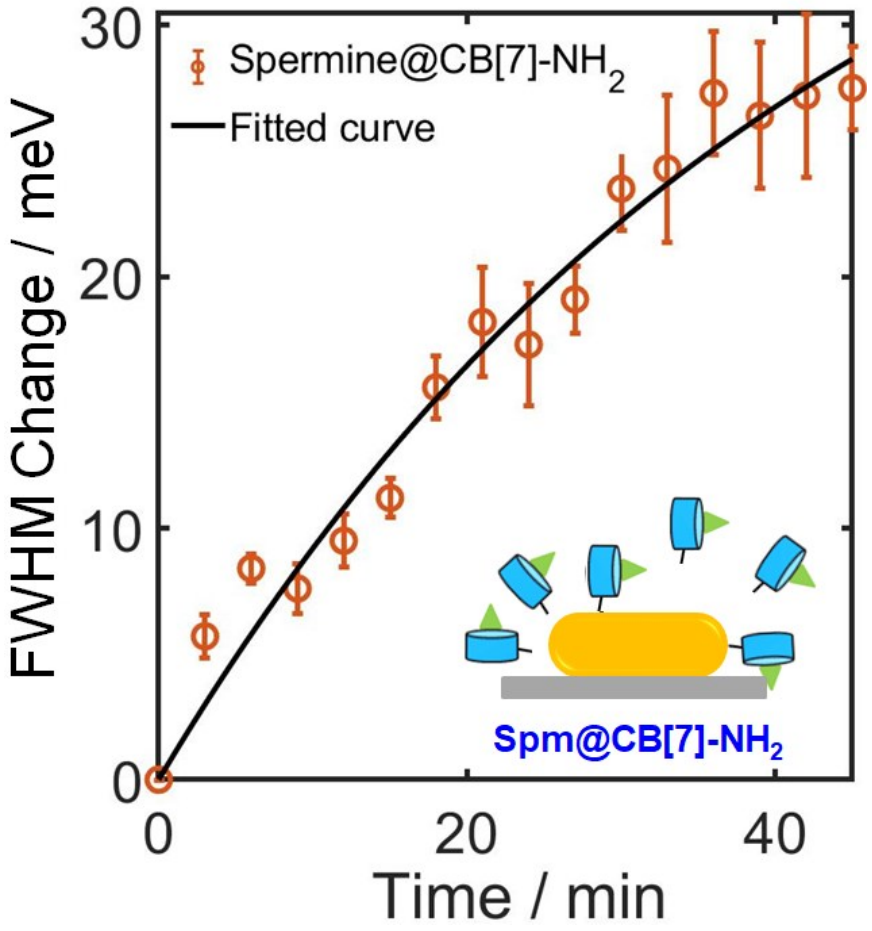

Fig. S19 Time dependence of the adsorption of spm@CB[7]-NH_2 observed *via* LSPR linewidth (or FWHM) broadening for single AuNRs. The scattering spectra of 50 single AuNRs were obtained repeatedly for a period of approximately 60 min and the LSPR linewidth $\Delta\Gamma$ was extracted with respect to the starting value. The fitted curves are shown as black. The presented kinetics of FWHM change (or CID) is an average of 50 single AuNRs and the error bars are their standard deviations.

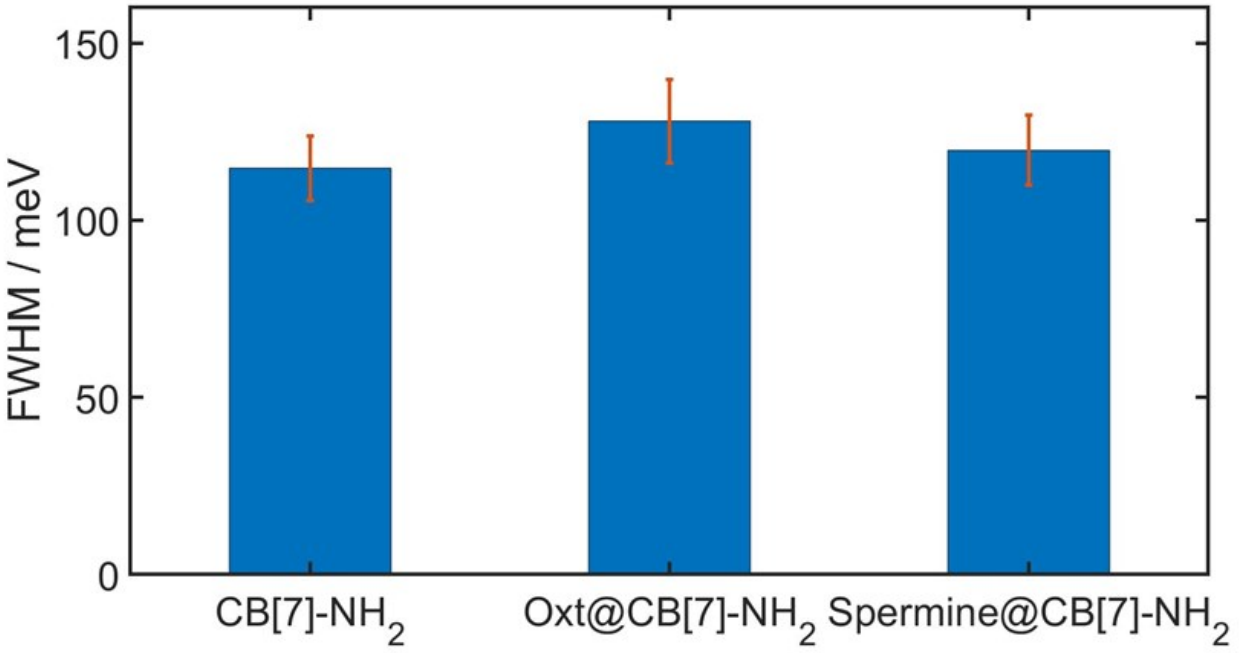

Fig. S20 Comparison of the linewidth broadening (or FWHM) induced by the adsorption of CB[7]-NH_2 (left), oxt@CB[7]-NH_2 (middle), and spm@CB[7]-NH_2 on the AuNR surfaces, under the same experimental conditions.

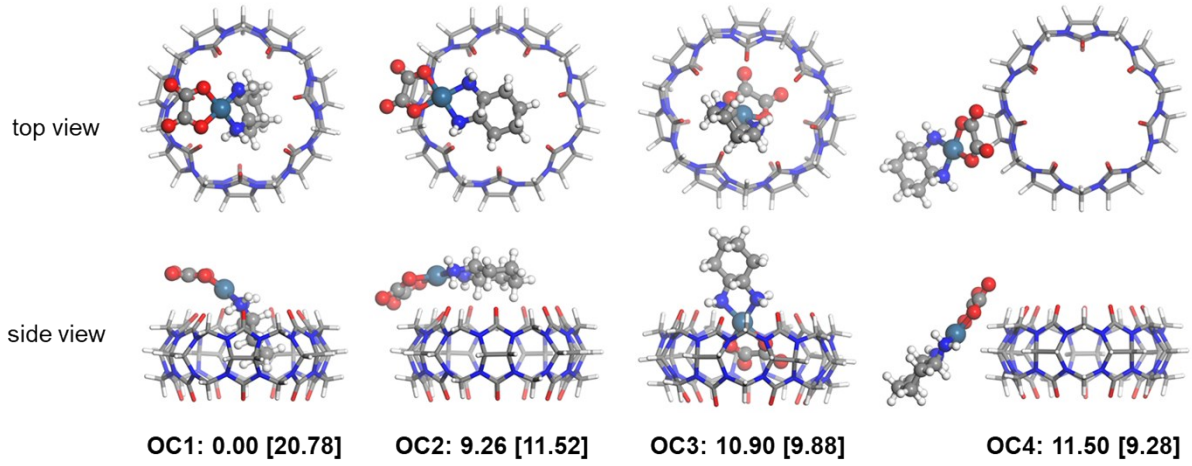

Fig. S21 Optimized local minimum structures and their relative energies [encapsulation energies = {E(CB[7]) + E(Oxt)} – E(Oxt@CB[7])] (in kcal/mol) for oxt@CB[7] (OC).

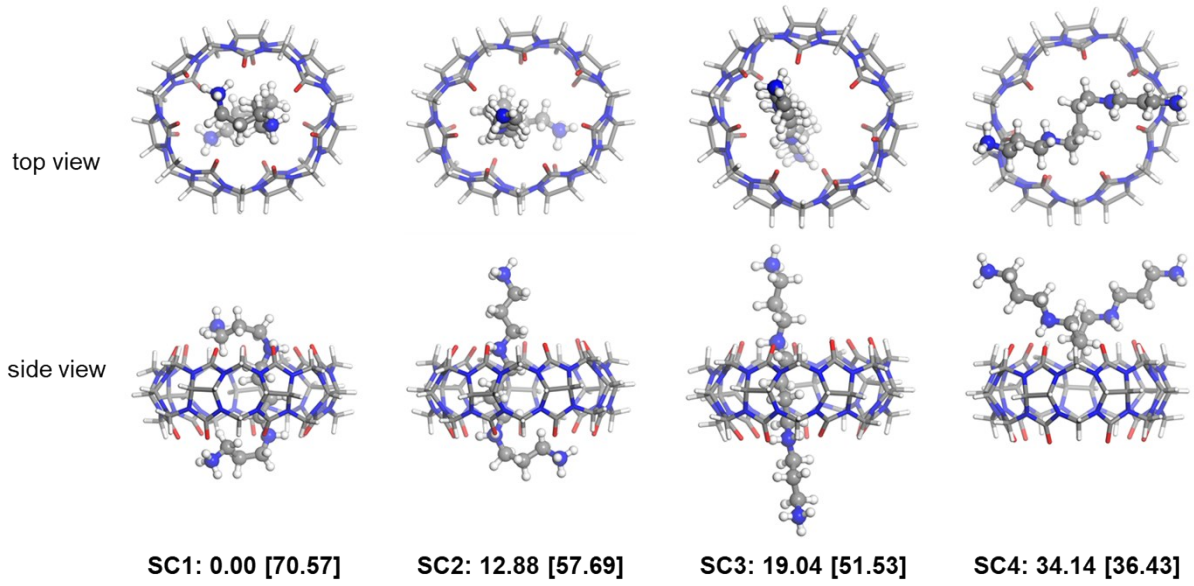

Fig. S22 Optimized local minimum structures and their relative energies [encapsulation energies = {E(CB[7]) + E(spermine)} – E(spermine@CB[7])] (in kcal/mol) for spermine@CB[7] (SC).

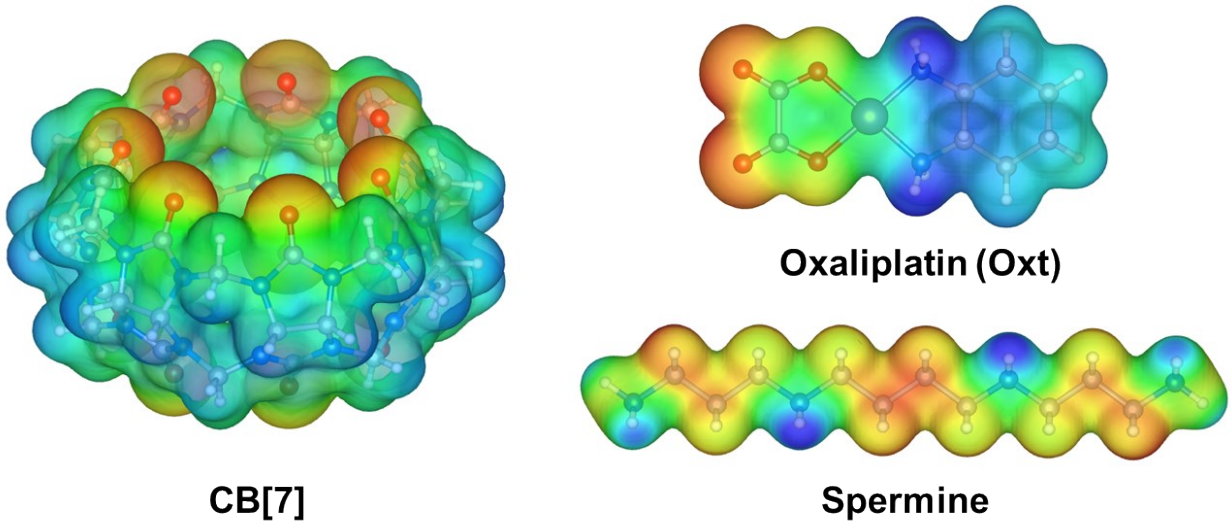

Fig. S23 Electrostatic potential (ESP) maps of CB[7], oxaliplatin, and spermine. Color scale from red to blue corresponds to negative to positive.

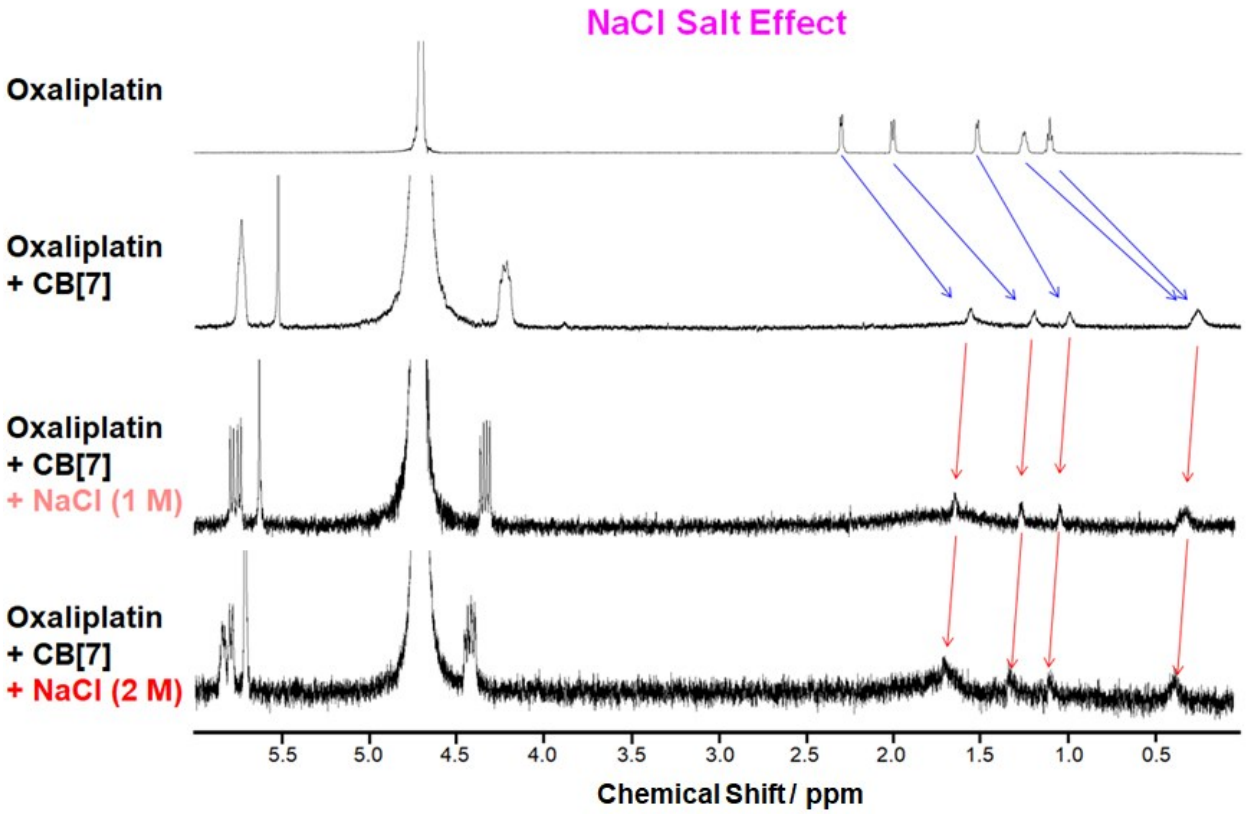

Fig. S24 The ^{1}H NMR spectroscopic measurements were performed to confirm the release of guest from its inclusion complex by the addition of NaCl. With the gradual increase in the concentration of NaCl, the NMR signals of the protons of 1,2-diaminocyclohexane on oxaliplatin shifted downfield toward the peak positions of oxaliplatin only, indicating the release of oxaliplatin from the CB[7] cavity

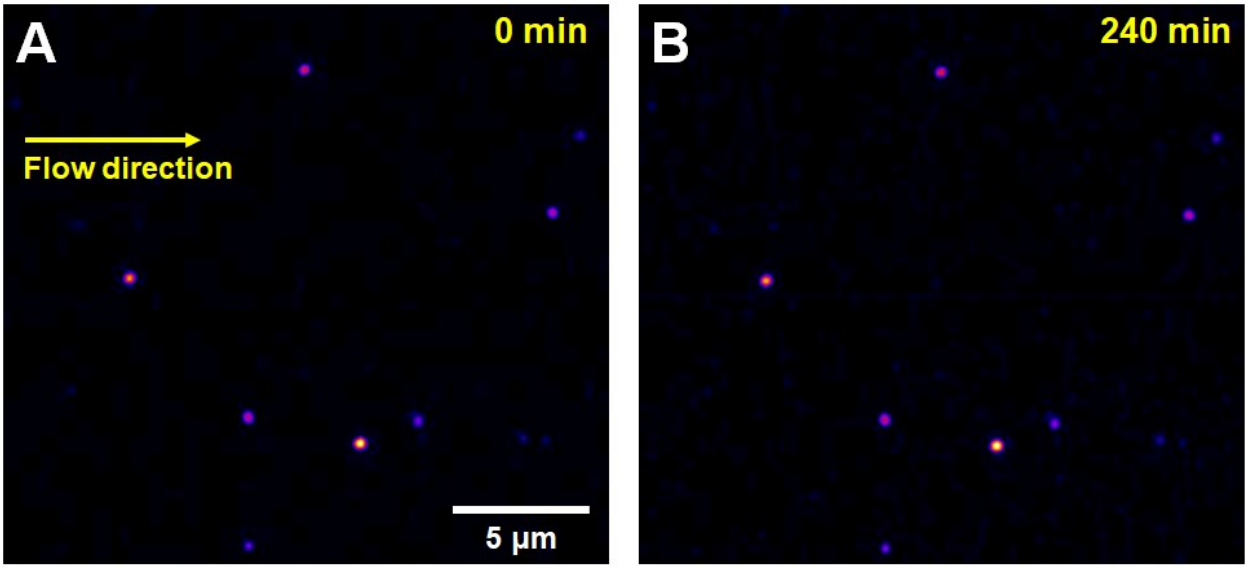

Fig. S25 Long-term stability of AuNRs fixed on a glass slide during the single-particle measurements in a flow cell. **(A)** DF scattering image of AuNRs before the single-particle measurements. **(B)** DF scattering image of same AuNRs after the experiments for 4 h in a flow cell.

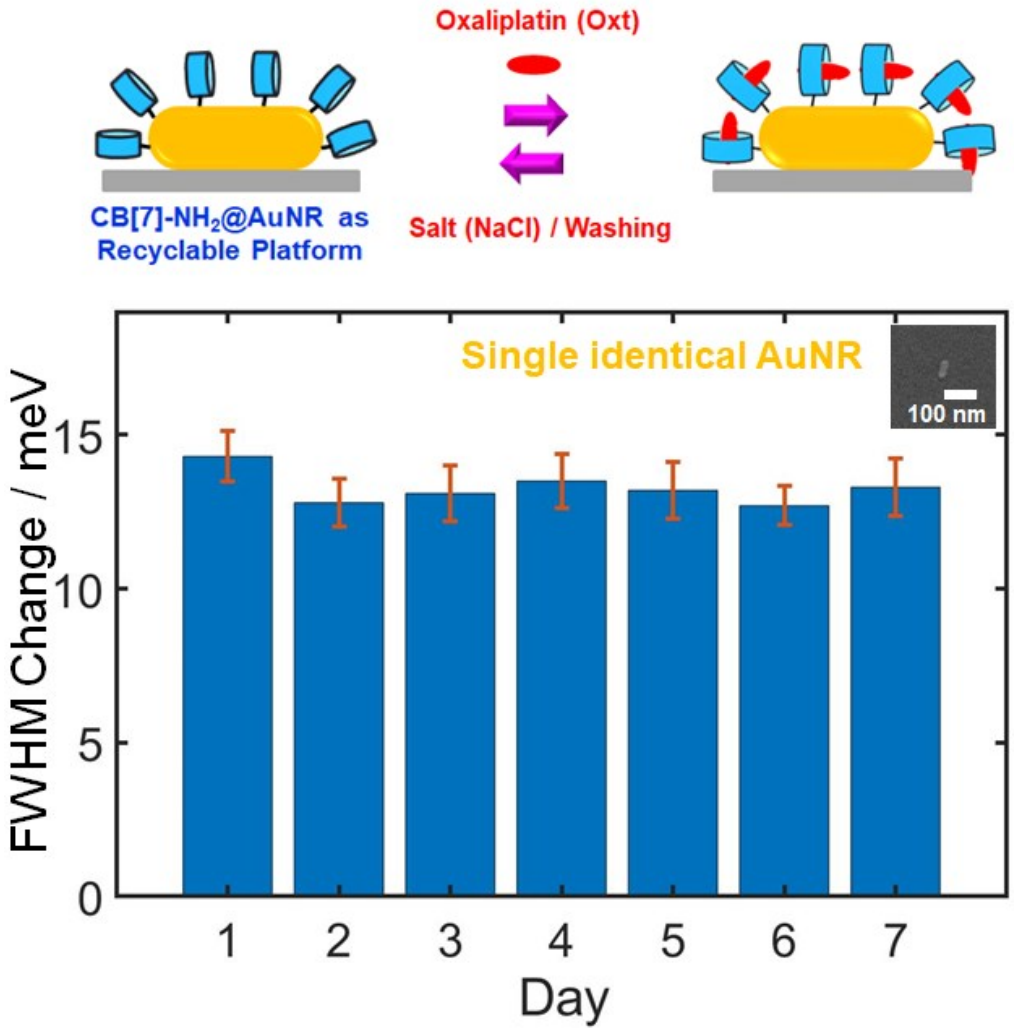

Fig. S26 The recyclability and reproducibility of CB[7]-NH_2@AuNR as a new platform for the CID investigations. Single-particle DF experiments were repeatedly performed for 7 consecutive days under the same experimental condition. Furthermore, we conducted 5 experiments a day under the same experimental condition to obtain the error bars. In this study, the equilibrium $\Delta\Gamma_{CID}$ values were obtained by fitting to a Langmuir adsorption process in the single AuNR.

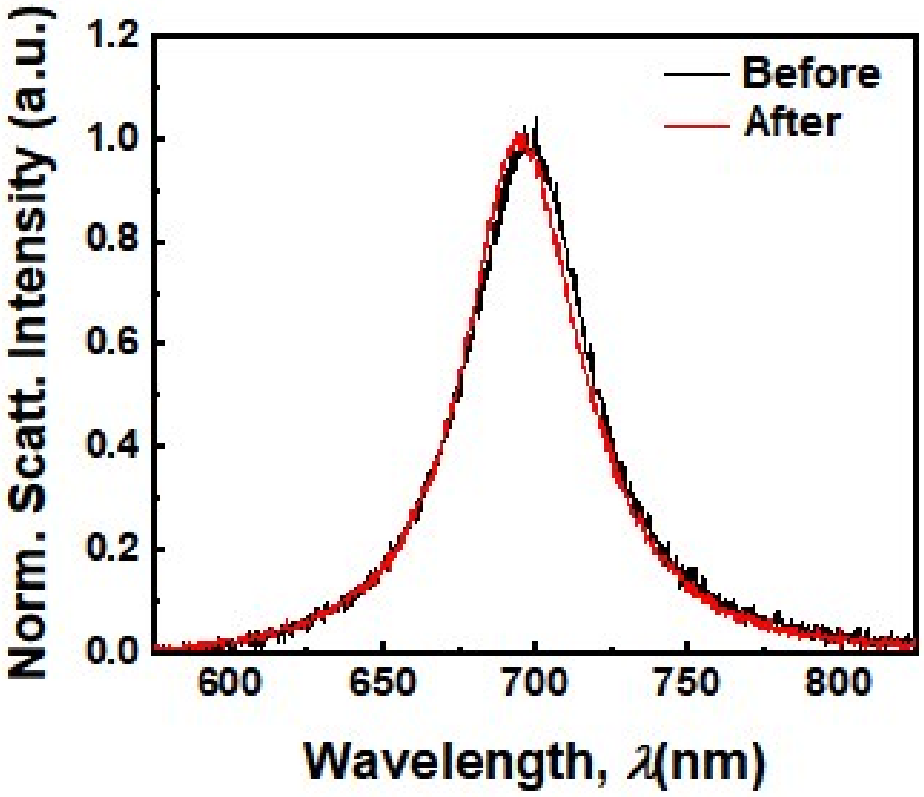

Fig. S27 Comparison of scattering spectra of single identical AuNR before and after the white light illumination. No noticeable spectral change was observed in single particle scattering spectrum obtained after the white light illumination for 4 h. The result supports that the shape transformation can be ruled out under our experimental conditions.